

Heterogeneous distribution of the dynamic source parameters of the 1999 Chi-Chi, Taiwan, earthquake

Wenbo Zhang, Tomotaka Iwata, Kojiro Irikura, Haruko Sekiguchi, Michel Bouchon

▶ **To cite this version:**

Wenbo Zhang, Tomotaka Iwata, Kojiro Irikura, Haruko Sekiguchi, Michel Bouchon. Heterogeneous distribution of the dynamic source parameters of the 1999 Chi-Chi, Taiwan, earthquake. Journal of Geophysical Research : Solid Earth, 2003, 108, 10.1029/2002JB001889 . insu-03607111

HAL Id: insu-03607111

https://insu.hal.science/insu-03607111

Submitted on 13 Mar 2022

HAL is a multi-disciplinary open access archive for the deposit and dissemination of scientific research documents, whether they are published or not. The documents may come from teaching and research institutions in France or abroad, or from public or private research centers.

L'archive ouverte pluridisciplinaire **HAL**, est destinée au dépôt et à la diffusion de documents scientifiques de niveau recherche, publiés ou non, émanant des établissements d'enseignement et de recherche français ou étrangers, des laboratoires publics ou privés.

Copyright

JOURNAL OF GEOPHYSICAL RESEARCH, VOL. 108, NO. B5, 2232, doi:10.1029/2002JB001889, 2003

Heterogeneous distribution of the dynamic source parameters of the 1999 Chi-Chi, Taiwan, earthquake

Wenbo Zhang, Tomotaka Iwata, and Kojiro Irikura
Disaster Prevention Research Institute, Kyoto University, Kyoto, Japan

Haruko Sekiguchi
Active Fault Research Center, Geological Survey of Japan, Tsukuba, Japan

Michel Bouchon
Laboratoire de Geophysique Interne et Tectonophysique, Université Joseph Fourier, Grenoble, France

Received 22 March 2002; revised 9 January 2003; accepted 6 February 2003; published 6 May 2003.

[1] The spatial and temporal distribution of the stress on the fault plane of the 1999 Chi-Chi, Taiwan, earthquake is calculated from kinematic inversion results using a three-dimensional finite difference method for solving the elastodynamic equations. We analyze the relations between stress and slip for all grid positions on the fault, and use these relations to infer the friction law for the rupture. The dynamic source parameters were also determined. Our results show that for most of the points on the fault, the relation between stress and slip was consistent with the slip-weakening law during the rupture process, especially for those points with large slip. However, consistency with the velocity-weakening law is not clear from the observed relation between stress and slip velocity. The distributions of the dynamic parameters on the fault are very heterogeneous. The peak value of the static stress drop is ~35 MPa. In general, high stress drop occurred in the areas with large slip. The estimated strength excesses are generally small suggesting that the tectonic shear stress had reached the level of the fault strength before the main shock. The slip-weakening distance D_c and the fracture energy G_c are proportional to the final slip. The aftershock activity correlates with the spatial distribution of dynamic source parameters. Usually, the aftershocks near the fault plane are concentrated in regions with small or negative static stress drop, and there were few aftershocks in regions which had large values of critical slip-weakening distance D_c. *INDEX TERMS:* 7209 Seismology: Earthquake dynamics and mechanics; *KEYWORDS:* dynamic source parameters, Chi-Chi earthquake, stress drop, slip weakening frictional law, slip weakening distance, strength excess

Citation: Zhang, W., T. Iwata, K. Irikura, H. Sekiguchi, and M. Bouchon, Heterogeneous distribution of the dynamic source parameters of the 1999 Chi-Chi, Taiwan, earthquake, *J. Geophys. Res.*, *108*(B5), 2232, doi:10.1029/2002JB001889, 2003.

1. Introduction

[2] Earthquake source processes are very complex at all scales. Well-recorded earthquakes, such as the 1992 Landers earthquake, the 1995 Kobe earthquake, the 1999 Chi-Chi earthquake and the 2000 Tottori earthquake, give seismologists the opportunity to investigate the source process in detail. Waveform inversion techniques have been widely applied to near source strong motions and more detailed kinematic source models have been obtained [*Hartzell and Heaton*, 1983; *Archuleta*, 1984; *Wald and Heaton*, 1994; *Ide et al.*, 1996; *Yoshida et al.*, 1996; *Sekiguchi et al.*, 2000; *Iwata et al.*, 2000a, 2000b]. These kinematic inversion results gave us the slip distributions on the fault planes. But for these kinematic models, there are some physical inconsistencies in the stress-slip relations compared to the real earthquake source process. In the kinematic models the rupture is assumed to propagate at a constant speed or within a certain range of speeds [*Peyrat et al.*, 2001], and the time-dependent slip function is the fundamental parameter. Questions about the physics of the rupture processes are not addressed. In fact, an earthquake is a dynamically propagating shear crack that radiates seismic waves and the stress variation on the fault plane is an indication of the dynamic behavior of earthquake rupture. As *Aki and Richards* [1980] pointed out, to understand the physical processes occurring in the source region, one must study stress-dependent material properties. That is, one examines the way in which material failure nucleates and spreads (e.g., over a fault plane), rapidly relieving stresses that had slowly risen (due to long-term tectonic processes) to exceed the strength of material in the source region. Dynamic simulations on earthquake rupture pro-

Copyright 2003 by the American Geophysical Union.
0148-0227/03/2002JB001889$09.00

cesses are the best way to investigate the physics of earthquakes.

[3] Since the pioneering work of *Quin* [1990], many papers have investigated the dynamic processes of earthquakes [*Fukuyama and Mikumo*, 1993; *Olsen et al.*, 1997; *Fukuyama and Madariaga*, 1998, 2000; *Madariaga et al.*, 1998; *Aochi et al.*, 2000; *Miyatake*, 2000; *Oglesby et al.*, 2000.]. In general, forces or stresses on fault planes are considered fundamental quantities in the dynamic models. An earthquake involves three main stages: (1) initiation of rupture, (2) frictional sliding during the rupture process, (3) and termination of the rupture. Laboratory experiments show that the relationship between sliding displacement and applied shear stress is not smooth. The dynamics of frictional sliding are very complex. How to describe the relationship during stage 2 is the goal of constitutive friction laws. The friction laws determine the fault behavior, and control the rupture processes. For dynamic simulation of the seismic source rupture process, the friction laws play an important role. For different earthquakes, the source rupture processes appear to be different. This diversity and complexity suggest that material properties controlling rupture evolution are spatially heterogeneous and may vary strongly for different earthquakes. Accordingly, understanding the prevailing friction laws and the relevant parameters could provide a unifying physical basis for understanding this variability and heterogeneity of the source processes. Two friction laws have been commonly used: the slip-weakening law [*Ida*, 1972; *Andrews*, 1976; *Day*, 1982.] and the velocity weakening law [*Carlson and Langer*, 1989; *Cochard and Madariaga*, 1994, 1996; *Fukuyama and Madariaga*, 1998]. Laboratory experiments of rock friction show that many materials become weaker with increasing slip and eventually enter the stable sliding mode. This behavior is known as slip weakening. Also some materials exhibit an inverse dependence of friction on slip velocity. This type of behavior is known as velocity weakening. Many studies have presented various friction laws based on laboratory experiments of rock friction in which frictional sliding is regarded as an analog to fault slip in natural earthquakes [*Dieterich*, 1978; *Dieterich et al.*, 1978; *Okubo and Dieterich*, 1984; *Ohnaka*, 1990; *Ohnaka and Shen*, 1999]. This is because direct measurements of stress at or near a fault are only possible at shallow depth and these results are difficult to reconcile with one of the friction laws. However, the scale of laboratory rock experiments is too small compared with a fault to apply the experimental results directly to actual earthquakes. Thus, we need to estimate the friction laws from the observed waveform data of actual events. In recent years, the detailed kinematic models of earthquake slip obtained for some large well-recorded events provide us the means to indirectly infer some of the characteristics of the stress field acting on earthquake faults. In this study, we will use a 3-D finite difference method (FDM) proposed by *Pitarka* [1999] under appropriate boundary conditions to directly solve the elastodynamic equations and calculate the stress spatiotemporal distribution over a fault plane from a kinematic inversion result. We apply this approach to study the dynamic source parameters of the 1999 Chi-Chi, Taiwan, earthquake and try to infer from the results some aspects of the dynamics of the rupture during this event, including friction laws.

2. Calculation Method and the Fault Model of the Chi-Chi Earthquake

[4] To determinate the stress field on the fault plane from the slip spatiotemporal distribution obtained by kinematic inversion, we used a 3-D finite difference method (FDM) presented by *Pitarka* [1999] to solve the following elastodynamic equations with appropriate boundary condition:

Equations of momentum conservation

$$\begin{cases} \partial_t v_x = b\left(\partial_x \tau_{xx} + \partial_y \tau_{xy} + \partial_z \tau_{xz} + f_x\right) \\ \partial_t v_y = b\left(\partial_x \tau_{xy} + \partial_y \tau_{yy} + \partial_z \tau_{yz} + f_y\right) \\ \partial_t v_z = b\left(\partial_x \tau_{xz} + \partial_y \tau_{yz} + \partial_z \tau_{zz} + f_z\right) \end{cases} \tag{1}$$

Stress-strain relations

$$\begin{cases} \partial_t \tau_{xx} = (\lambda + 2\mu)\partial_x v_x + \lambda\left(\partial_y v_y + \partial_z v_z\right) \\ \partial_t \tau_{yy} = (\lambda + 2\mu)\partial_y v_y + \lambda(\partial_x v_x + \partial_z v_z) \\ \partial_t \tau_{zz} = (\lambda + 2\mu)\partial_z v_z + \lambda(\partial_x v_x + \partial_z v_z) \\ \partial_t \tau_{xy} = \mu\left(\partial_y v_x + \partial_x v_y\right) \\ \partial_t \tau_{xz} = \mu(\partial_z v_x + \partial_x v_z) \\ \partial_t \tau_{yz} = \mu\left(\partial_z v_y + \partial_y v_z\right) \end{cases} \tag{2}$$

In these equations, (ν_x, ν_y, ν_z) are the particle velocity components; (τ_{xx}, τ_{yy}, τ_{zz}, τ_{xy}, τ_{xz}, τ_{yz}) are the stress components; (f_x, f_y, f_z) are the body force components; b= $1/\rho$ is the buoyancy, ρ is the density; λ and μ are the Lamé coefficients; and the ∂_x, ∂_y, ∂_z, and ∂_t, are shorthand representations of the differential operators ∂/∂_x, ∂/∂_y, ∂/∂_z, and ∂/∂_t. In this method, the fourth-order staggered grid expressions for discrete spatial differential operators and the second-order approximate for time derivatives are used to model wave propagation in 3-D elastic media.

[5] Figure 1 shows the fault model of the 1999 Chi-Chi earthquake. The fault model is the same as the one used by *Iwata et al.* [2000b] for kinematic inversion analyses. Details of the kinematic model will be given in section 3. The fault model has a curved plane and is divided into subfaults. In the FDM coordinate system, we adopt x axis is the direction N93°E, y axis is the direction N3°E, and z axis is direction down. During the calculation, we used four boundary conditions. The first set of boundary conditions is the free surface condition, which is the zero-stress formulation [*Graves*, 1996], $\tau_{zz}\,|_{z=0} = \tau_{xz}\,|_{z=0} = \tau_{yz}\,|_{z=0} = 0$. The second set of boundary conditions is the continuity condition at each layer interface included in the medium, that is, the continuity of stresses and displacements. The third set of boundary conditions is an absorbing boundary condition [*Clayton and Engquist*, 1977] for the side and bottom boundaries that attenuates elastic waves reflected back from these artificial side and bottom boundaries of the model

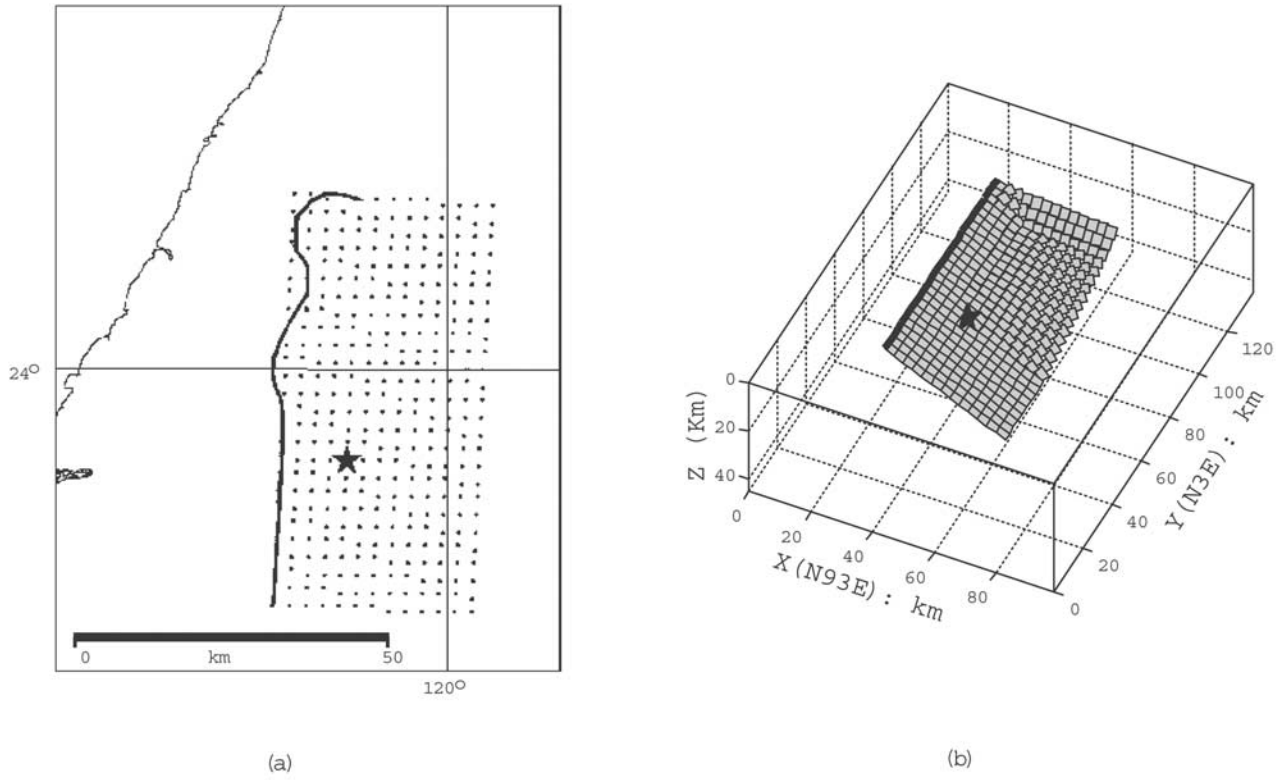


Figure 1. (a) Map showing the surface breaks of the Chi-Chi earthquake (thick curve) with the projection of the fault model onto the free surface (dot is the center of each subfault). The star is the epicenter. (b) The geometry of the fault model of the Chi-Chi earthquake [*Iwata et al.*, 2000b]. The star is the hypocenter.

space. The fourth set of boundary conditions is for the points on the fault plane. For these points, we used the kinematic inversion results as the fault plane boundary conditions. The kinematic inversion results gave us the slip distributions on each subfault. Each subfault is like a point source with arbitrary focal mechanism; the moment tensor components can be represented as an equivalent distribution of body force couples centered at the grid point corresponding to each subfault. We used the moment tensor source formulation proposed by *Graves* [1996], which use a distribution of body forces are added to the individual components of velocity.

[6] In this work, we only consider the shear stress along the direction of slip on each subfault. The appendix describes detail how to calculate the stress along the slip direction from the six stress components (τ_{xx}, τ_{yy}, τ_{zz}, τ_{xy}, τ_{xz}, τ_{yz}) for each subfault.

3. Stress Field on the Fault Plane of the 1999 Chi-Chi, Taiwan, Earthquake

[7] The 21 September 1999 M7.6 Chi-Chi, Taiwan, earthquake is one of the strongest earthquakes in history in Taiwan, and a large number of strong motion records were obtained during this event. The fault rupture during this earthquake is very complex. A single fault plane segment is not sufficient to describe the fault. *Iwata et al.* [2000b] used a nonplanar fault model as shown in Figure 1 and 31 station data (velocity 0.05–0.5 Hz) to successfully invert the kinematic source model of this earthquake. Figure 2 is the final slip distribution obtained on the fault [*Iwata et al.*, 2000b]. As shown in Figure 2, strong slip heterogeneity is observed. Large slips are observed in the northern part and along the shallowest part of the fault. The directions and magnitudes of the inverted slip vectors in the shallow part of the fault roughly coincide with the observations of surface rupture. In this study, we used Iwata et al.'s kinematic inversion results to analyze the stress distribution on the fault by the method described in section 2. As shown in Figure 1, the fault has a curved surface. When it is projected onto the free surface, it is 78 km in length and 39 km in width. The fault is divided into 26 × 13 subfaults, and each subfault occupies a 3 km × 3 km area when it is projected onto the free surface. Since the fault plane is curved, each subfault has different strike and dip. However, most of the subfaults have a strike direction of N3°E and a dip angle of 29°. We used the same one-dimensional model of velocities and densities in the source region (Table 1) as used in the kinematic inversion by *Iwata et al.* [2000b]. In order to satisfy the stability condition for FDM, and also in order to represent the fault geometry adequately, the grid sizes used in our FDM calculation were chosen as $\Delta x = \Delta y = 0.60$ km, and $\Delta z = 0.33$ km.

[8] Figure 3 shows the spatial and temporal distribution of stress on the fault plane inferred from the kinematic inversion results. From the computed stress time histories on the fault we can estimate dynamic parameters, such as strength excess, dynamic stress drop and static stress drop.

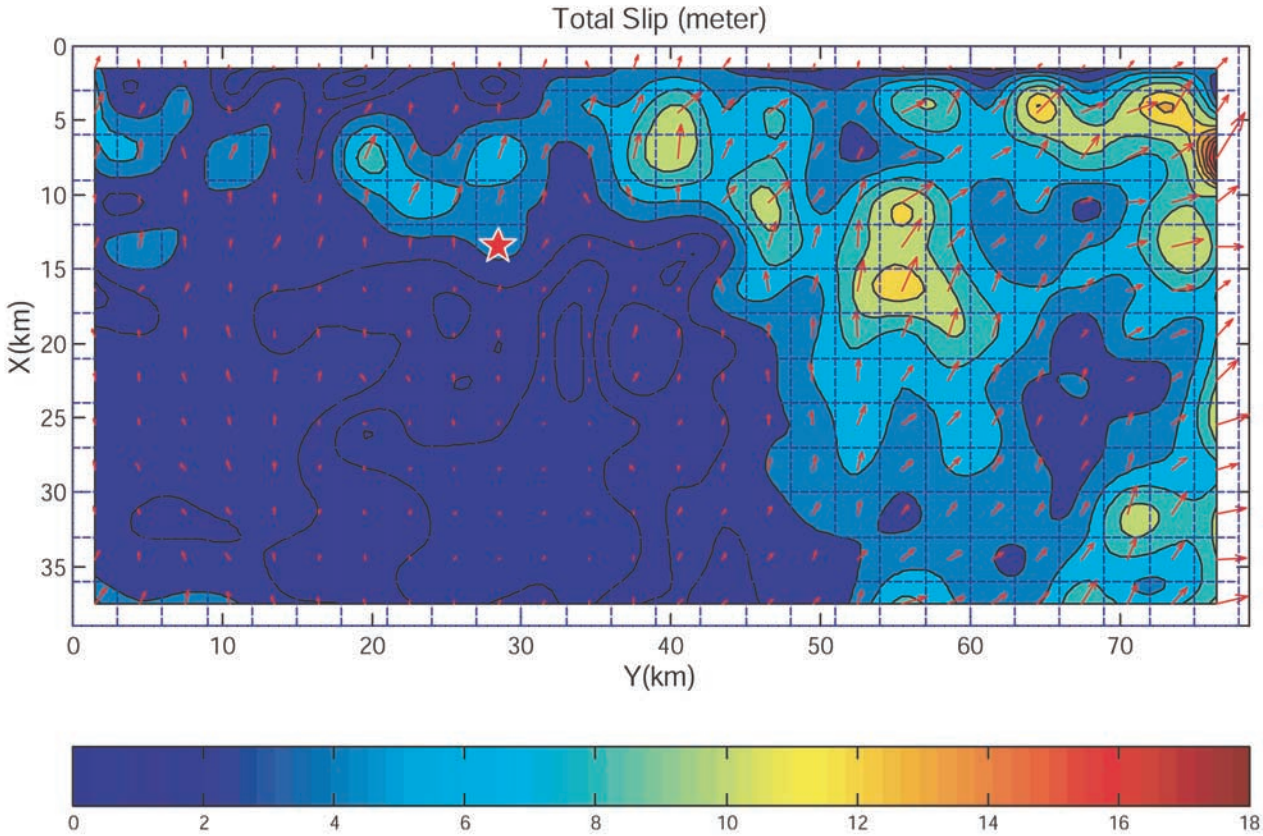


Figure 2. Distribution of the final slip on the fault [*Iwata et al.*, 2000b]. The horizontal component of the final slip is contoured, and the star is the hypocenter.

Figure 4 shows a typical time history of stress on the fault and illustrates how to estimate the three parameters from a time history of stress. As shown in Figure 4, the shear stress increases above the initial stress level σ_0 and reaches a peak σ_y just before rupture. Then the stress drops to a minimum level σ_f, before increasing slightly again to its final static value σ_s. The strength excess $\Delta\tau_y$ is defined as the amount of stress increase necessary to make the fault slip, i.e., $\Delta\tau_y = \sigma_y - \sigma_0$, the dynamic stress drop $\Delta\tau_d$ corresponds to the largest drop from the initial shear stress level during the rupture process, i.e., $\Delta\tau_d = \sigma_0 - \sigma_f$, while the static stress drop $\Delta\tau_s$ measures the change in stress produced by the earthquake, i.e., $\Delta\tau_s = \sigma_0 - \sigma_s$. Since we do not know the absolute values of the initial stress field on the fault and seismic waves are only sensitive to the stress change, the estimated dynamic parameters are relative values. The relation of slip and stress at each grid point of the fault can be used to study the friction laws during the rupture of this earthquake.

4. Friction Laws and Dynamic Parameters of the Chi-Chi Earthquake Friction Law

[9] The time histories of slip and stress on the fault plane of the Chi-Chi earthquake afford an opportunity to study the friction laws that governed the rupture process of an earthquake. *Ide and Takeo* [1997] were the first to investigate friction laws from data for a real earthquake (the 1995 Kobe earthquake). Their results show that for most points on the fault plane of the 1995 Kobe earthquake, the slip weakening law was followed during the rupture process, and the slip weakening rate in the shallow parts was significantly smaller than those in the deeper parts. It was not clear if velocity weakening behavior was observed. In this study, we examined the relationships between stress and slip, and between stress and slip rate on the Chi-Chi earthquake fault; tried to obtain the friction laws as well as the dynamic parameters.

[10] Figure 5 shows a typical slip-dependent (slip-weakening) and a typical rate-dependent (velocity-weakening) friction law. The corresponding dynamic parameters are also shown in Figure 5. In Figure 5a, $G_c = (\sigma_y - \sigma_s) \times D_c/2$ is the fracture energy for the slip-weakening model. Figure 6 shows our results for the shear stress as a function of slip (Figure 6a) and the shear stress as a function of slip rate (Figure 6b) at some grid points on the fault. Our results are similar to those obtained by *Ide and Takeo* [1997]. In our case, the behavior of most of the grid points on the fault

Table 1. Velocity Structure Used in This Calculation

Depth, km	V_p, km/s	V_s, km/s	Density, kg/m^3	Q_p	Q_s
0.00	2.88	1.55	2000.	200.	100.
0.91	3.15	1.70	2050.	400.	200.
1.91	4.37	2.50	2300.	500.	250.
3.70	5.13	2.85	2400.	500.	250.
8.00	5.90	3.30	2600.	550.	270.
13.0	6.21	3.61	2700.	600.	300.
17.0	6.41	3.71	2750.	700.	350.
25.0	6.83	3.95	2800.	800.	400.
30.0	7.29	4.21	3000.	1000.	500.

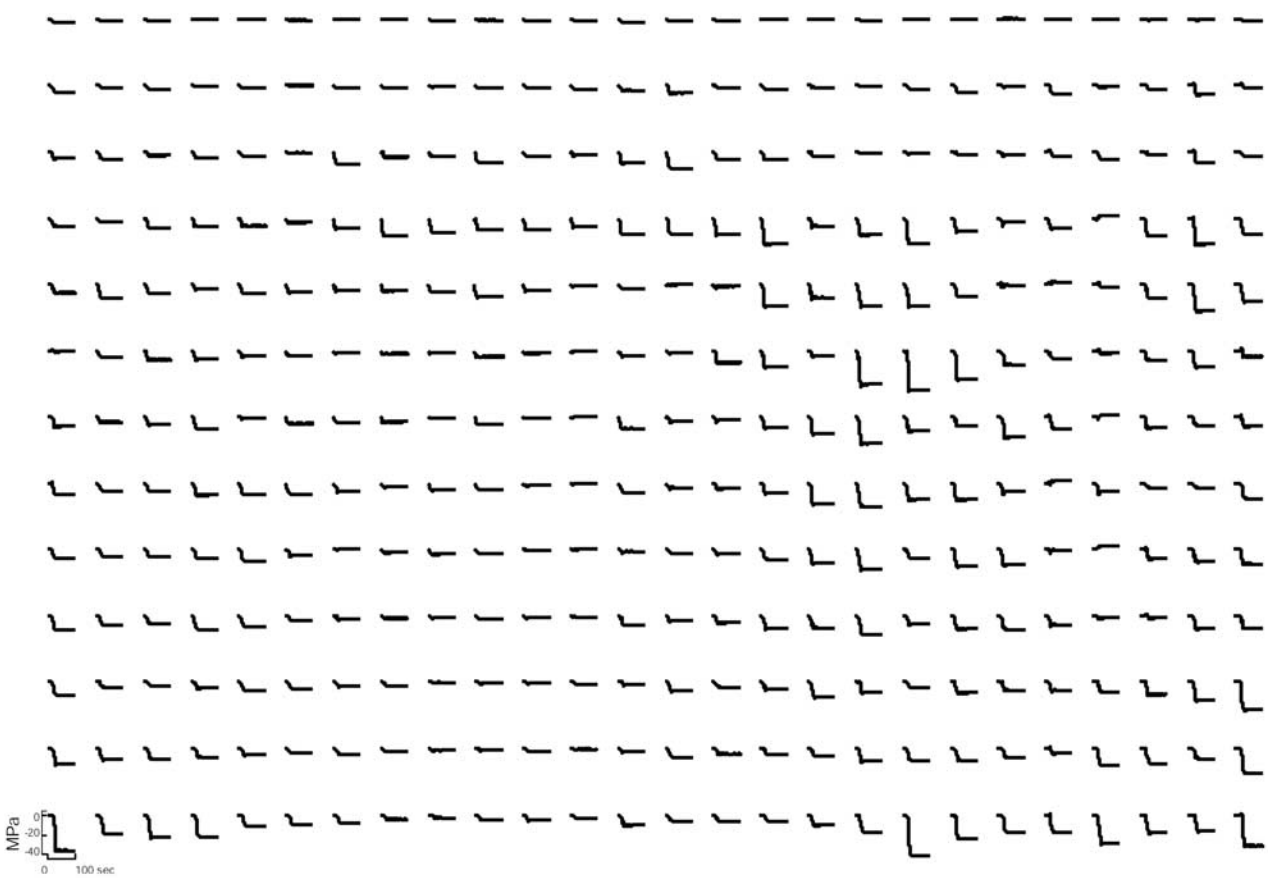


Figure 3. Spatial and temporal distribution of stress on the fault inferred from the kinematic inversion result.

is consistent with a slip weakening law, especially for those with a large slip. However, in our results, the slip weakening rate does not significantly vary with depth. *Bouchon et al.* [1998] also obtained the same result for the 1995 Kobe earthquake. In Figure 6a, except those points near the free surface (the three dark solid lines, depth is ~2 km), the slip weakening rate of the other points at different depth is nearly same. The free surface condition we used in FDM makes the stress of points at near the free surface change slowly. Accordingly the slip weakening rate of these points is smaller than for points far from the free surface. From Figure 6b, we cannot determine whether the behavior follows the velocity-weakening law or not. As shown in Figure 6b, when rupture starts, the stress decreases with the slip rate increasing, which is the behavior of a velocity-weakening law, but after the peak value of slip rate, the stress still decreases with the slip rate decreasing, which is not the behavior of a velocity-weakening law. This is because that velocity weakening occurred initially, but the fault did not recover strength as long as it was still moving. *Ide and Takeo* [1997] obtained the same result. They pointed out that although the velocity weakening in the slip accelerating process is visible, this is trivial and easily predicted by slip weakening behavior. On the other hand, velocity weakening behavior is unclear in the slip decelerating process. Also, it is difficult to determine the slip at low rate by waveform inversion. This is because of the poor resolution of the data at high frequency and the constraints imposed on the model to perform the inversion. We need a high resolution of the slip model to check velocity-weakening laws in the future. In this study, we determined the dynamic parameters based on a simple slip-weakening law as described by

Initial condition: $D = 0$, $\sigma < \sigma_y$

$$\sigma = \begin{cases} \sigma_y + (\sigma_s - \sigma_y)\dfrac{D}{D_c} & 0 < D \le D_c \\ \sigma_s & D > D_c \end{cases} \tag{3}$$

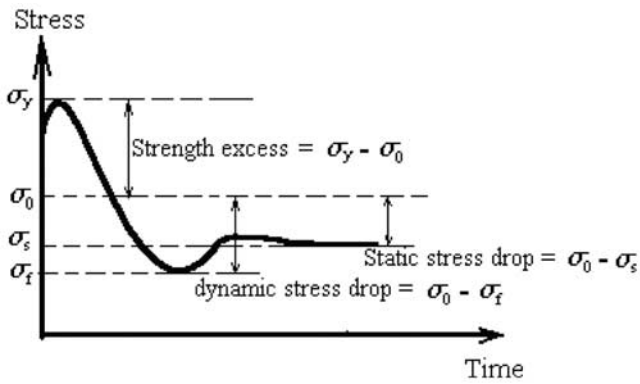


Figure 4. Schematic illustration of determination of the strength excess, static stress drop, and dynamic stress drop.

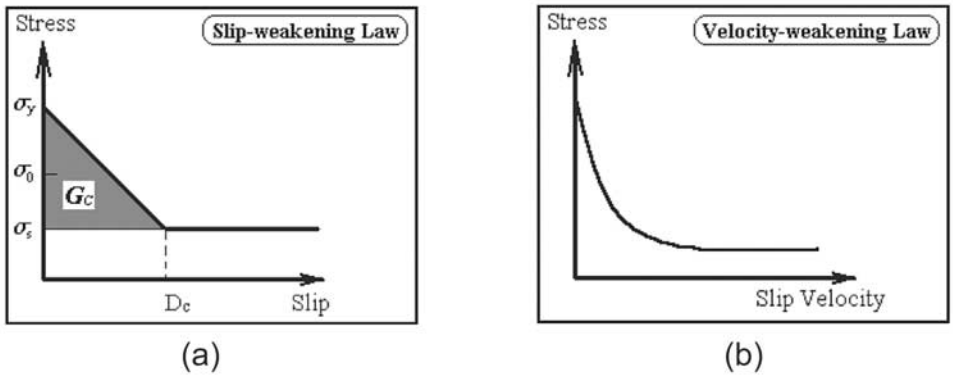


Figure 5. (a) A simple and typical slip-weakening friction law. (b) A simple and typical velocity-weakening friction law.

where D is the slip, D_c is the critical slip-weakening distance, σ is the shear stress, and σ_s, σ_y are the static stress level and yield stress level, respectively. In this model, the crack tip serves as a stress concentrator [*Ita*, 1972; *Ohnaka and Yamashita*, 1989]. If the stress at the crack tip exceeds a critical value σ_y, then the crack begins to rupture and the stress drops to the dynamic frictional value σ_f as the fault slips locally to release the stress. After that, the stress usually increases again and finally reaches the static value σ_s as the rupture stops. Figure 4 shows this process.

4.1. Stress Drop

[11] Figure 7 shows snapshots of the distributions of slip and stress on the fault plane of the Chi-Chi earthquake.

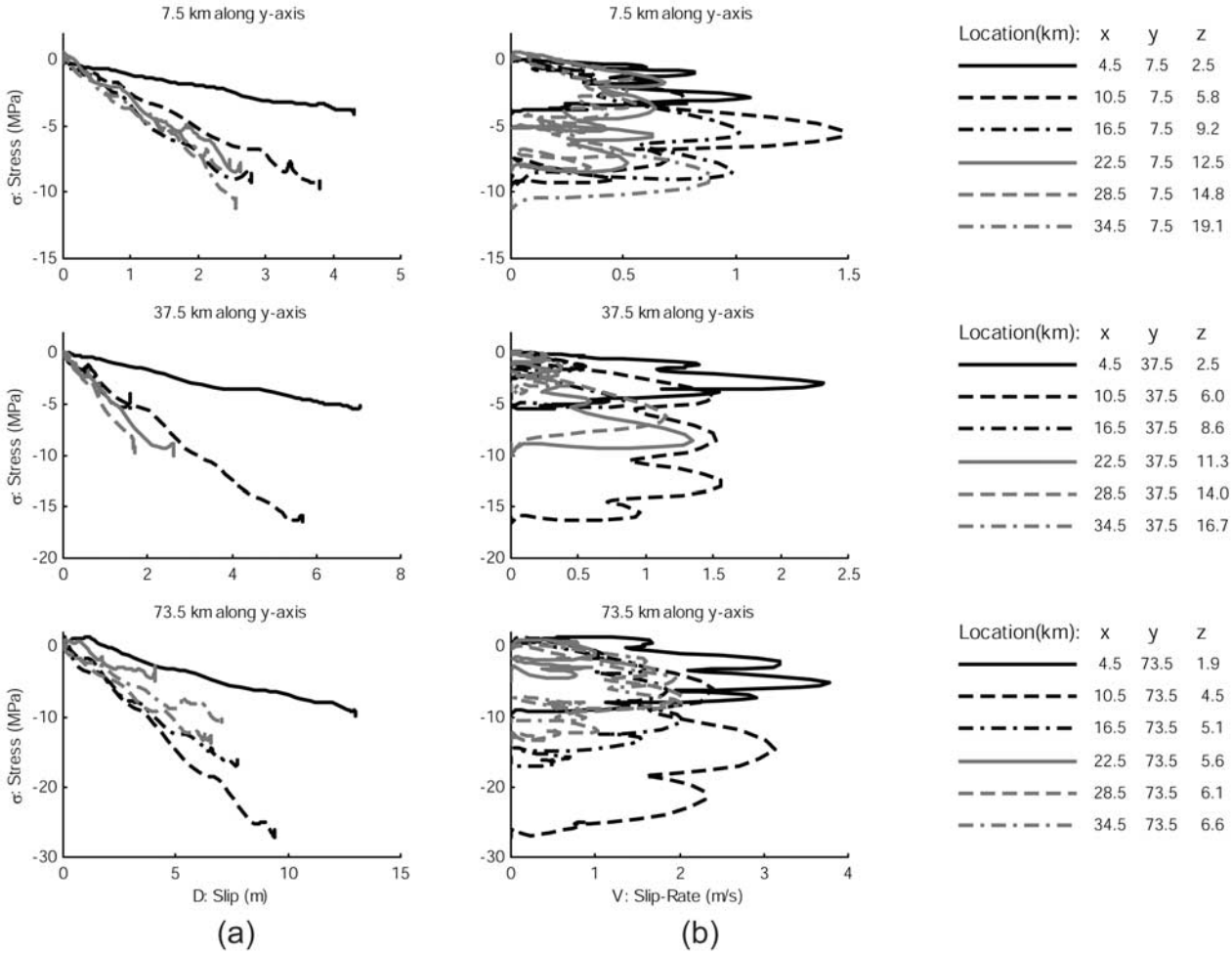


Figure 6. (a) Shear stress as a function of slip and (b) shear stress as a function of slip rate at some grid points on the fault plane. The locations of these points are shown in right.

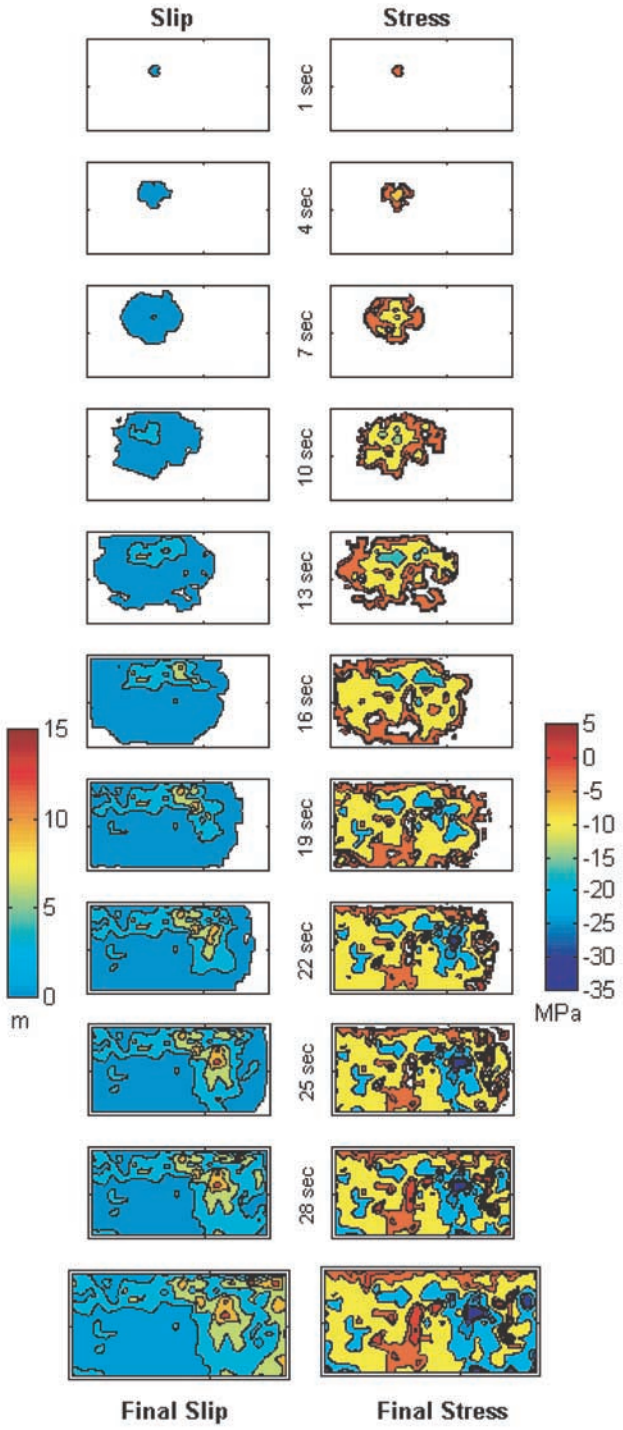


Figure 7. Snapshots of the distribution of slip and stress on the fault plane of the Chi-Chi earthquake.

Figure 8 shows the spatial distribution of stress drop (static and dynamic) on the fault plane. As Figures 7 and 8 show, the process of stress release is similar to the slip process, and the distribution of the stress drop is very heterogeneous. The largest stress drop did not occur in the hypocentral area, but in the northern part. There, the peak value of static stress drop reaches ~35 MPa and the peak value of dynamic stress drop reaches ~40 MPa. The stress drop distribution correlates with the final slip distribution (Figure 2). In general, large stress drop occurs around areas with a large slip. From Figure 8, we notice that there are very large stress drops at the bottom of the fault; this is an unexpected phenomenon for the dynamic simulation. The most likely causation of this phenomenon is because of the kinematic inversion results. As Figure 2 shows, some of these areas also have quite large slip. The stresses are an artifact due to the fact that slip does not go to zero at the borders of the fault model (Figure 2). Stress, in theory, will become infinite at the borders of the fault. We will check this phenomenon in our future dynamic simulation of the ground motion.

[12] The spatial distribution of dynamic stress drop is very similar with that of static stress drop, with amplitude values ~10 to 40% higher. The dynamic stress drop is positive everywhere, indicating that after rupture, the shear stress always drops below its initial level, and eventual increases slightly again to its finial static values.

4.2. Strength Excess

[13] Figure 9 shows the distribution of strength excess on the fault. The amount of stress increase necessary for the fault rupture varies depending on the position on the fault. The strength excess is only a fraction of a megapascal around the hypocenter, so the rupture starts easily from there. The estimated strength excesses are generally small, suggesting that the tectonic shear stress had reached close to the level of the fault strength before the earthquake over a major portion of the fault. The several exceptions are some points in the northern part of the fault, their strength excesses reach ~3 MPa. From the viewpoint of dynamic rupture, these points with large strength excess will delay the rupture propagation. In Figure 9, we overlaid the rupture starting time of the kinematic model. From Figure 9, we see that the kinematic model shows rupture delay in the middle depths of the northern part, but failed in the other parts. This is a defect of the kinematic model; during the kinematic inversion, the technique of multitime window linear waveform inversion procedure by *Hartzel and Heaton* [1983] was used and the rupture velocity for each time window was assumed as 2 km/s. This means the rupture was constrained to propagate within a certain range of speeds. Because of this, the kinematic model can not reveal some characteristics of source rupture process.

4.3. Critical Slip-Weakening Distance D_c

[14] Another important parameter in the slip-weakening model is critical slip-weakening distance D_c. D_c is defined as the slip displacement required for the local strength in the breakdown zone behind the rupture front to degrade to a residual friction stress level. This critical slip displacement is related to the physical state of the fault and controls the evolution of stress toward its residual value when the fault sliding velocity suddenly changes [*Guatteri*, 2001]. How to estimate D_c is still under investigation. Several methods have been proposed to estimate the value of D_c [*Ide and Takeo*, 1997; *Guatteri and Spudish*, 2000; *Pulido and Irikura*, 2000; *Ohnaka*, 2000; *Zhang et al.*, 2001; *Mikumo et al.*, 2003]. *Mikumo et al.* [2003] presented an approach to estimate the critical slip-weakening distance D_c based on the relation between the breakdown time of shear stress, T_b, and the time of peak slip velocity, T_{pv}. Figure 10 explains this

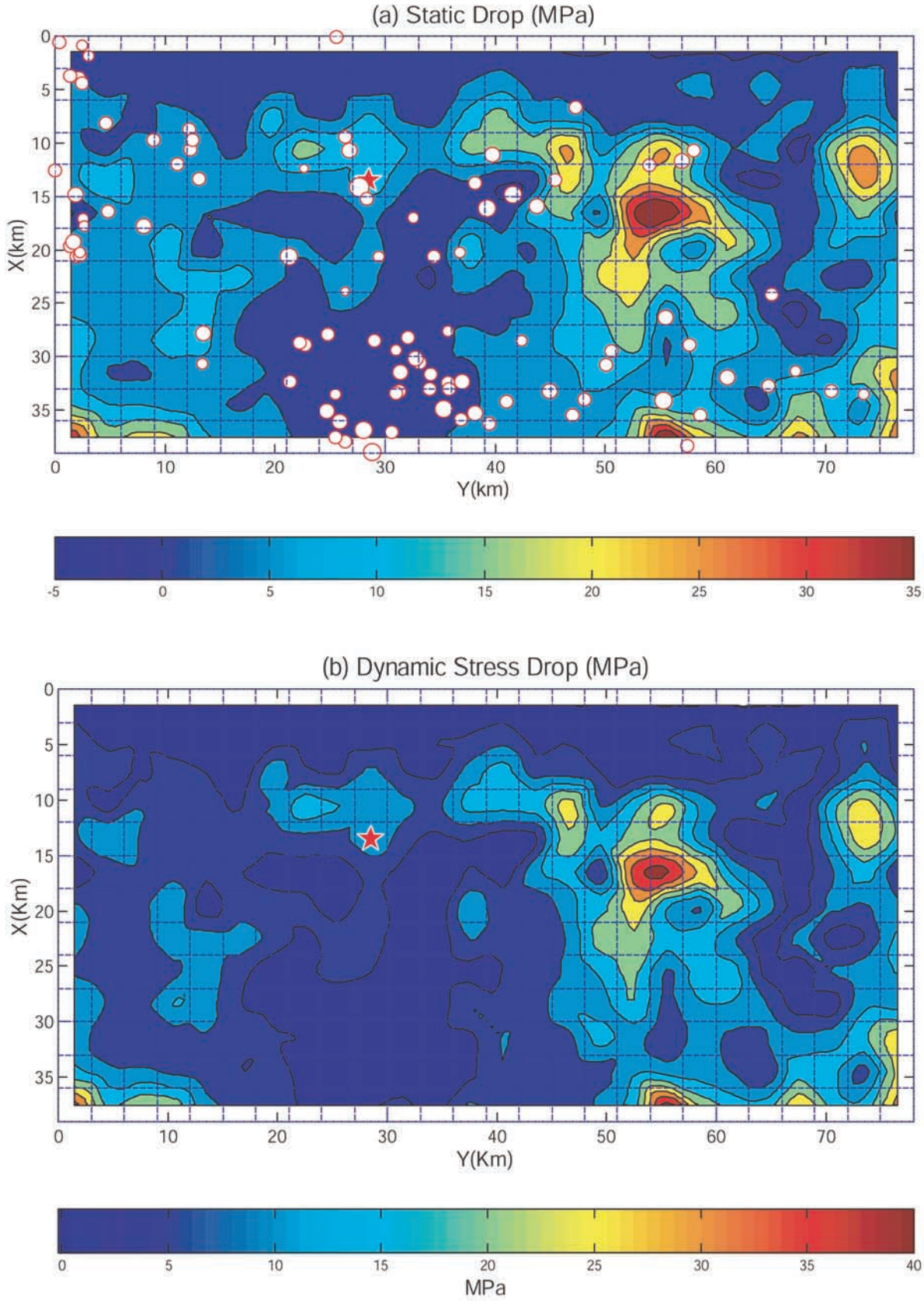


Figure 8. Distribution (a) of static stress drop and (b) dynamic stress drop on the fault. The red star is the hypocenter. In Figure 8a, the hypocenters of 96 early aftershocks are also plotted. These aftershocks occurred near the fault.

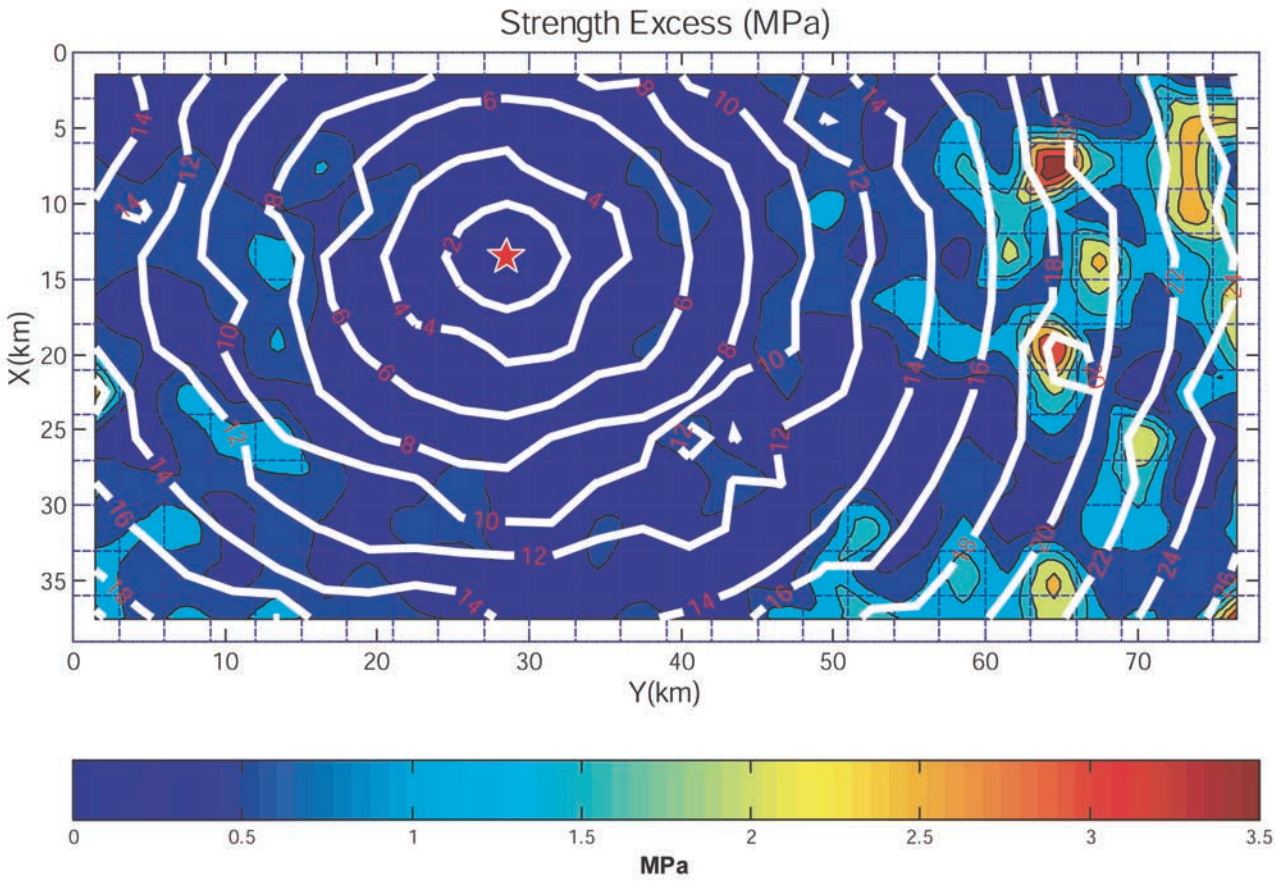


Figure 9. Distribution of strength excess on the fault plane with the distribution of kinematic rupture time (white lines).

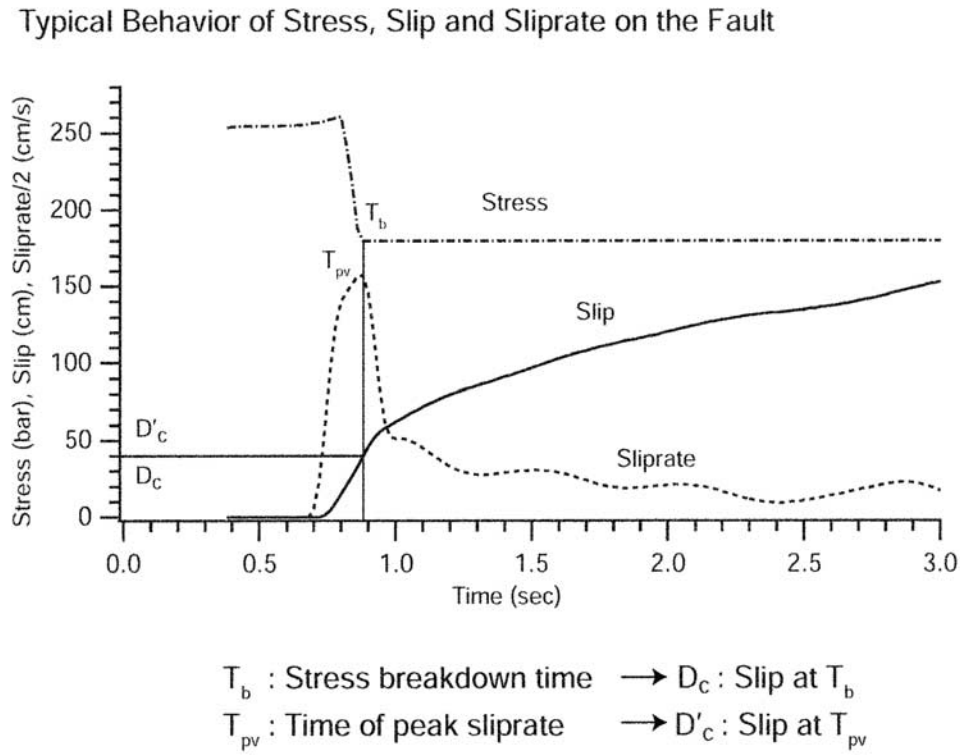


Figure 10. Schematic illustration of determination on the critical slip-weakening distance D_c [*Mikumo et al.*, 2003].

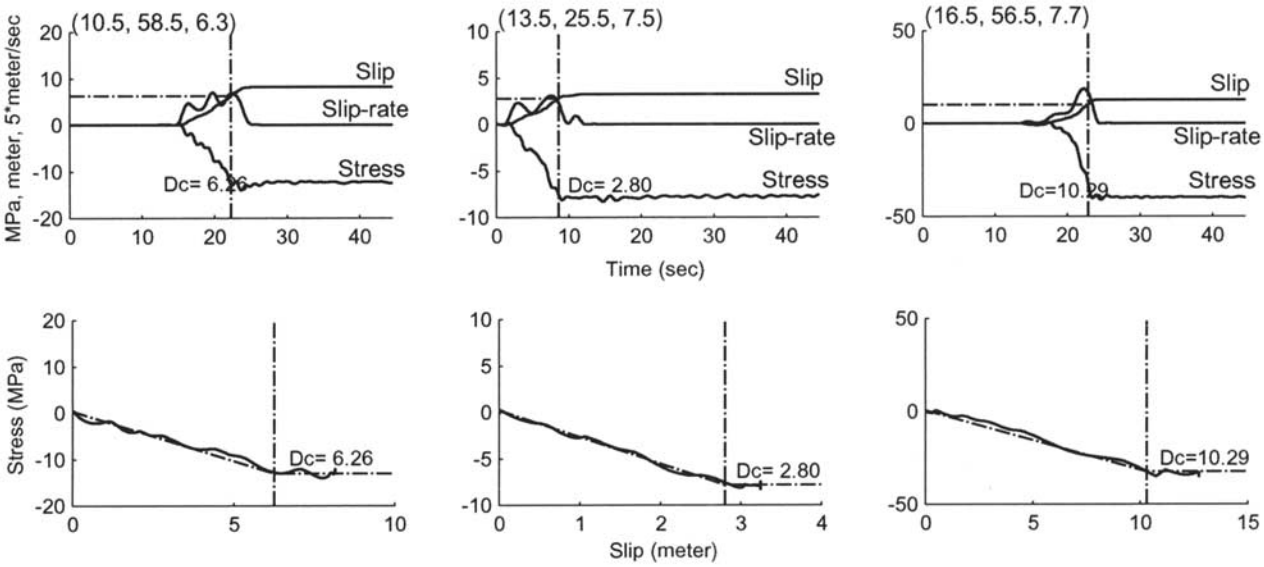


Figure 11. Illustration of estimation D_c for three points on the Chi-Chi fault by the approach of *Mikumo et al.* [2003]. The locations of the three points are shown on the top.

method. From results of numerical simulations and some theoretical background of this method, they concluded that D_c can be estimated with reasonable accuracy as the slip displacement at the time of peak slip velocity T_{pv} if T_b and T_{pv} are very close to each other. The value of D_c estimated from this method is independent of fracture energy G_c. *Guatteri and Spudish* [2000] found that from the estimates of waveform inversion results, there is a trade-off between strength excess and slip-weakening distance and only fracture energy can be estimated stably. In this study, we applied the approach proposed by *Mikumo et al.* [2003] to estimate D_c for those points when $T_b \approx T_{pv}$. However, there are still some points with T_b quite different from T_{pv}. For these points, we estimated the D_c based on the relation between stress and slip as shown in Figure 5a. Figure 11 illustrates estimation D_c for three points on the fault by the approach of *Mikumo et al.* [2003]. As shown in the figure, in our case, the results of this approach accord with the definition of $D_c$when $T_b \approx T_{pv}$. We also calculated the fracture energy for each subfault and obtained G_c from 10^5 to 10^8 J/m^2; these values are consistent with previous estimates for other earthquakes, which range from 10^2 to 10^8 J/m^2 [*Husseini, et al.*, 1975; *Aki*, 1979; *Beroza and Spudich*, 1988]. Figure 12 presents our results for the distribution of critical slip-weakening distance D_c on the fault plane of the Chi-Chi earthquake. In our case, D_c and G_c correlate with the final slip D_{final}. Figure 13 shows the relations between of D_c, G_c and the final slip D_{final}. As shown in Figure 13, in general, the slip weakening distance D_c, and the fracture energy G_c, is proportional to the final slip, i.e., $D_c \propto D_{\text{final}}$ and $G_c \propto D_{\text{final}}^{2.2}$.

[15] We should point out that because of the resolution of the kinematic inversion, for some locations it is difficult to determine the slip weakening distance D_c, especially for those points with a very small slip. Also, because of the effects of spatial and temporal smoothing constraints applied in kinematic inversion problem, the critical slip-weakening distance D_c estimated from the kinematic inversion model is likely to be large [*Ide and Takeo*, 1997; *Guatteri and Spudish*, 2000]. Our values of D_c can be considered as an upper bound estimate since we are using a kinematic model that was determined in a low and narrow frequency band (0.05–0.5 Hz).

4.4. Relation Between Seismic Activity and Dynamic Source Parameters

[16] Several attempts have been made to investigate the relation between seismic activity and the spatial distributions of the dynamic source parameters [*Marone and Scholz*, 1988; *Scholz*, 1988; *Bouchon*, 1997; *Ide and Takeo*, 1997; *Guatteri and Spudish*, 2000; *Zhang et al.*, 2001], and it has been found that aftershock seismic activity correlates to the spatial distributions of the dynamic source parameters. In this section, we selected 96 aftershocks from the 146 early aftershocks occurring in the first one and a half days after the main shock (from 1750 LT on 20 September to 2400 LT on 21 September 1999) to check the relation between aftershock seismic activity and the spatial distributions of the dynamic source parameters. These 96 early aftershocks occurred near the fault.

[17] In Figure 8a, we overlaid the hypocenters of the 96 early aftershocks of the Chi-Chi earthquake onto the spatial distribution of the static stress drop on the fault. As shown in Figure 8a, most of the aftershocks happened in the regions of the fault where static stress drop was small or negative. One interpretation is that, after the main shock, the regions with large static stress drop became areas of low level of tectonic stress and thus were much more stable. On the other hand, the level of tectonic stress remained high for the regions with small or negative static stress drop after main shock, and this made them prone to aftershock activity. However, in the northern shallow part of the fault, there were few aftershocks though static stress drop was also very small or negative in these areas. This paucity of

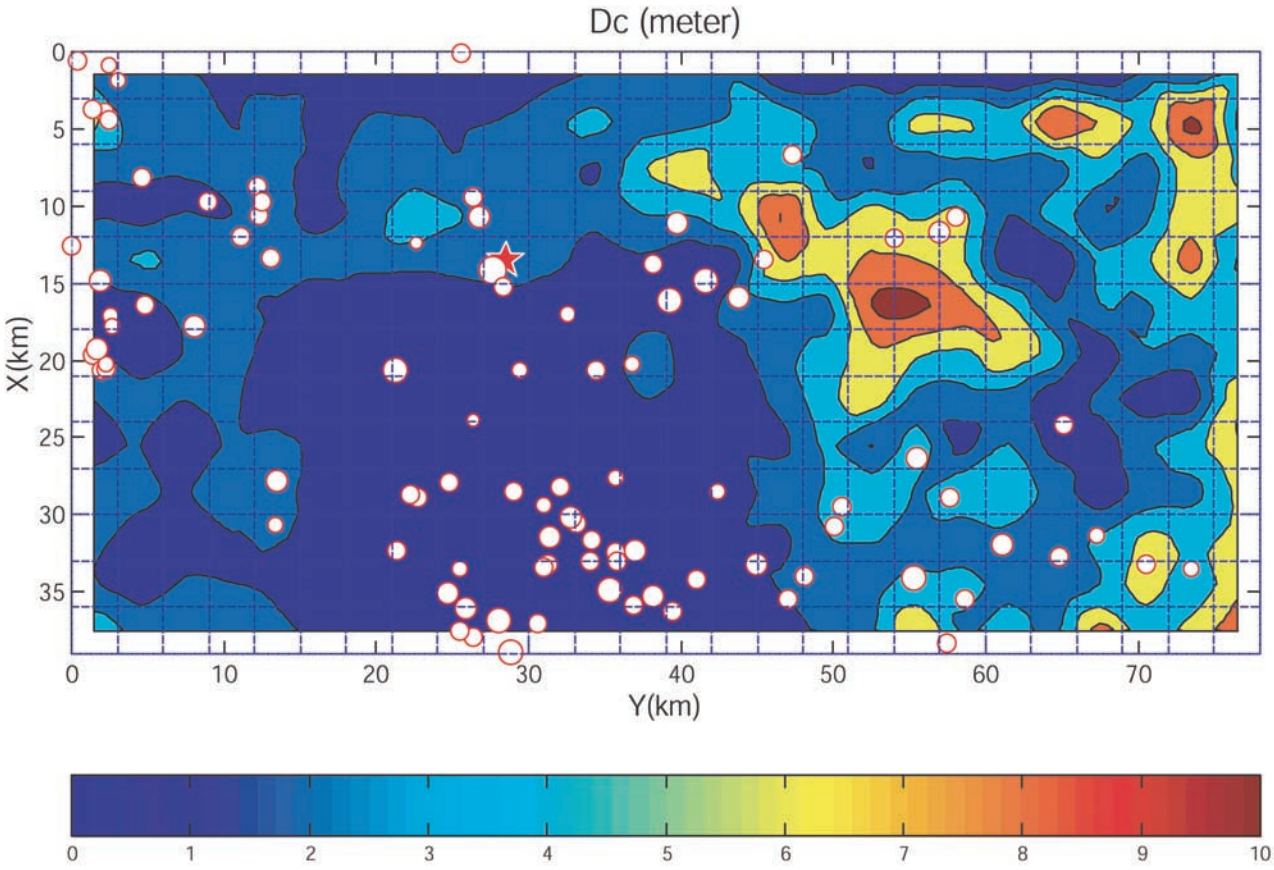


Figure 12. Distribution of the slip-weakening distance D_c on the fault with the hypocenters of 96 early aftershocks which happened near the fault.

seismic activity can be explained by the spatial distribution of critical slip-weakening distance D_c. In Figure 11, we overlaid the hypocenters of the 96 early aftershocks onto the spatial distribution of the critical slip-weakening distance D_c. In our case, larger values for D_c are found in several places in the northern part of the fault. *Scholz* [1988] indicated that if the critical slip distance D_c is too large, the fault will be stable and will not generate earthquake. Thus large values of D_c will prevent the seismic nucleation process and there will be reduced aftershock activity in such regions. Our result has proven this. As shown in Figure 11, there were very few aftershocks in the northern part of fault which have larger values of D_c.

5. Conclusions

[18] Stress evolution is estimated from the kinematic inversion results on the entire plane of the Chi-Chi earth-

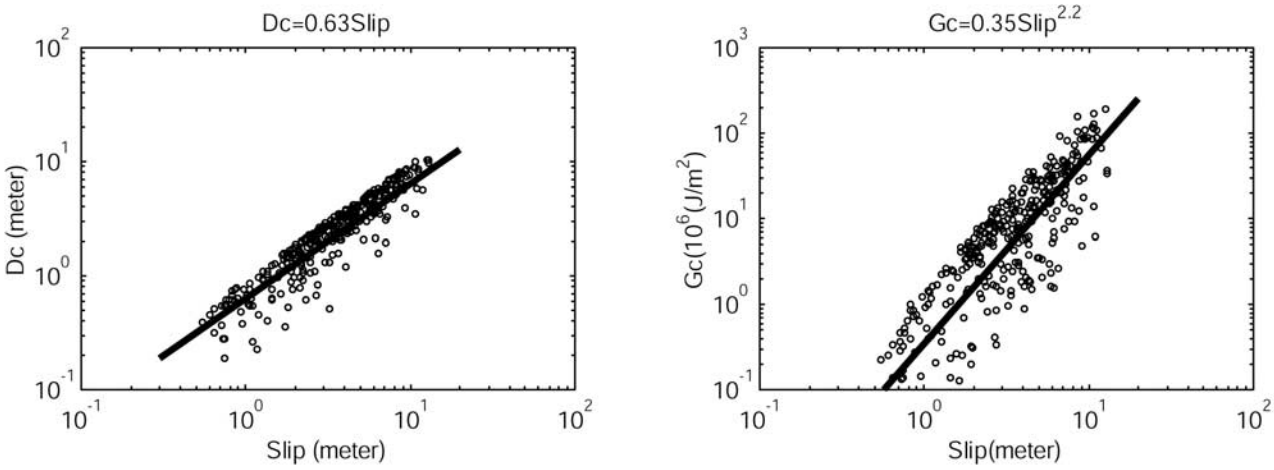


Figure 13. Slip-weakening distance D_c versus slip and the friction energy G_c versus slip on the fault.

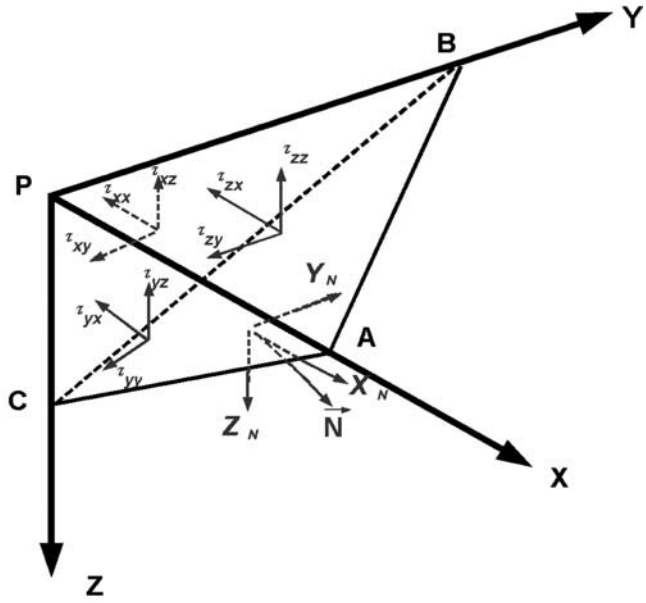


Figure A1. A small tetrahedron PABC around the center of a subfault.

quake fault. The relations between stress and slip, stress and slip rate on the fault, shows that most locations on the fault plane followed the slip-weakening model during the Chi-Chi earthquake rupture. The applicability of the velocity-weakening law is not conclusive. Our results show that the distributions of the dynamic parameters on the fault are very heterogeneous. The stress drop varies greatly over the fault and its distribution has a strong correlation with the final slip distribution. Large stress drops occur around areas with large slip. The large stress drop at the bottom boundary of the fault, which is an unexpected phenomenon for the dynamic simulation, this is probably because of the kinematic inversion results. The estimated strength excesses are generally small suggesting that the tectonic shear stress had reached near the level of the fault strength before the main shock. Concerning the slip-weakening distance D_c, which is a very important parameter in the slip-weakening model, our result shows that D_c is proportional to the final slip. The aftershock activity is related to the spatial distribution of dynamic source parameters. Usually, the aftershocks which occurred near the fault plane concentrated in regions with small or negative static stress drop. Large values of critical slip-weakening distance D_c will prevent the seismic nucleation process and there will be reduced aftershock activity in such regions. There indeed were few aftershocks in regions which had large values of critical slip-weakening distance D_c.

[19] We should point out that the inference of a fault constitutive relation requires good resolution in the interval of time and space. Our results are based on the kinematic inversion results, and we did not examine the question of resolution in this study. Because of the effects of spatial and temporal smoothing constraints applied in kinematic inversion problems, the estimated dynamic source parameters in this research may have some biases. Higher resolutions of kinematic models as well as improved inversion schemes are needed to further investigate the constitutive laws governing friction during real earthquakes. Nevertheless, even with the poor resolution, our results can be considered as a lower bound estimate for stress drop and strength excess and an upper bound estimate for critical slip-weakening distance.

Appendix A

[20] In the FDM calculation, we obtain the six stress components (τ_{xx}, τ_{yy}, τ_{zz}, τ_{xy}, τ_{xz}, τ_{yz}) for each of the subfaults. Here we will explain how to calculate the shear stress along the slip direction from the six stress components for each of subfaults.

[21] Assume P is the center of a subfault. We select a small tetrahedron PABC as shown as Figure A1, which is constituted by four planes, the plane PAB parallel to axis the x-y plane, the plane PBC parallel to axis the y-z plane, the plane PAC parallel to axis the x-z plane, and the plane ABC parallel to the plane of the subfault. When this tetrahedron is small, the plane ABC will trend to point P, and the stresses on the plane ABC are equal to the stresses on this subfault. Assuming **N** is the normal vector of ABC plane:

$$N_x = \cos(\mathbf{N}, \mathbf{x}) = l, \quad N_y = \cos(\mathbf{N}, \mathbf{y}) = m, \quad N_z = \cos(\mathbf{N}, \mathbf{z}) = n. \tag{A1}$$

If the area of triangle ABC is ΔS, then the areas of triangle PBC, PAV, and PAB are $l\Delta S$, $m\Delta S$, and $n\Delta S$, respectively. (X_n, Y_n, Z_n) are the stress components when the stress on the plane of ABC is projected onto the axes. For the condition of force balance along $x$axis, $\sum F_x = 0$, we get

$$X_n \Delta s - \tau_{xx} l \Delta s - \tau_{yx} m \Delta s - \tau_{xz} n \Delta s = 0$$

so,

$$X_n = \tau_{xx} l + \tau_{yx} m + \tau_{xz} n$$

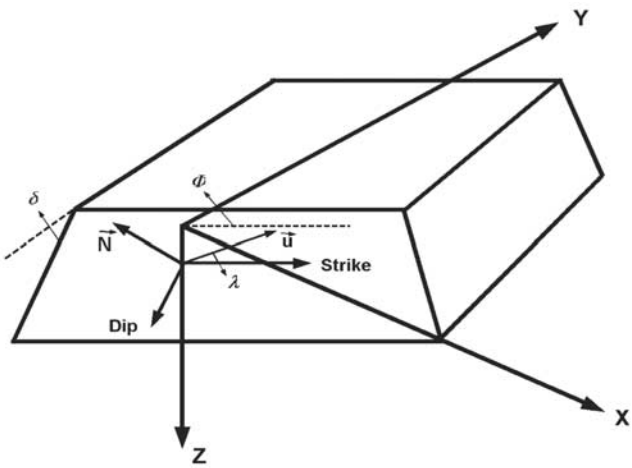


Figure A2. Definition of the fault orientation parameters and slip direction.

Y_n, Z_n can be obtained by the same way. Thus

$$\begin{cases} X_n &= m\tau_{xx} + l\tau_{yx} + n\tau_{zx} \\ Y_n &= m\tau_{yx} + l\tau_{yy} + n\tau_{zy} \\ Z_n &= m\tau_{xz} + l\tau_{yz} + n\tau_{zz} \end{cases} \quad \text{(A2)}$$

Figure A2 defines of the fault orientation parameters (strike ϕ, dip δ, rake λ), and slip direction; ϕ is measured clockwise round from the y axis (in our FDM, N3°E), δ is measured down from the horizontal, and λ is the angle between strike direction and slip. In Figure A2, N is fault normal:

$$\mathbf{N} = \sin\ \delta\ \cos\ \phi\mathbf{x} - \sin\delta\ \sin\phi\mathbf{y} - \cos\ \delta\mathbf{z},$$

i.e., $l = \sin\ \delta\ \cos\ \phi$, $m = -\sin\ \delta\ \sin\ \phi$, $n = -\cos\ \delta$. Projecting the stresses (X_n, Y_n, Z_n) from the x-y-z coordinates onto the strike-dip-normal coordinates, we obtain the stress components in strike, dip and normal:

$$\begin{cases} \tau_{strike} &= \sin\phi X_n + \cos\phi Y_n \\ \tau_{dip} &= \cos\phi\cos\delta X_n - \sin\phi\cos\delta Y_n + \cos\delta Z_n \\ \tau_{normal} &= \cos\phi\sin\delta X_n - \sin\phi\sin\delta Y_n - \cos\delta Z_n \end{cases} \quad \text{(A3)}$$

Then projecting the τ_{strike}, τ_{dip} on the slip direction we obtain the shear stress along the slip direction:

$$\tau_{\text{slip}} = \tau_{\text{strike}}\cos\lambda - \tau_{\text{dip}}\sin\lambda. \quad \text{(A4)}$$

[22] **Acknowledgments.** We are grateful to Dudley Andrews and Raul Madariaga and to an anonymous reviewer for their valuable comments, suggestions and critiques. We wish to thank A. Pitarka for his kindly providing us his FDM program, and thank to Huey-Chu Huang for offering the hypocenters of the aftershocks. This study was supported by a Grant-in-Aid for Science Research 11792026, from the Ministry of Education, Science, Sports and Culture of Japan. This study was partially supported by Special Coordination Fund (2000–2004) of MEXT, titled "Study on the master model for strong ground motion prediction toward earthquake disaster mitigation," and Grants-in-Aid for Scientific Research in priority area (B) 11209201 (PI. T. Iwata).

References

Aki, K., Characterization of barriers on an earthquake fault, *J. Geophys. Res.*, *84*, 6140–6148, 1979.

Aki, K., and P. G. Richards, *Quantitative Seismology: Theory and Methods*, 799 pp., W. H. Freeman, New York, 1980.

Andrews, D. J., Rupture propagation with finite stress in antiplane strain, *J. Geophys. Res.*, *81*, 3575–3582, 1976.

Aochi, H., E. Fukuyama, and M. Matsu'ura, Spontaneous rupture propagation on a non-planar fault in 3-D elastic medium, *Pure Appl. Geophys.*, *157*, 2003–2027, 2000.

Archuleta, R., A faulting model for the 1979 Imperial Valley earthquake, *J. Geophys. Res.*, *89*, 4559–4589, 1984.

Beroza, G. C., and P. Spudich, Linearized inversion for fault rupture behavior: application to the 984 Morgan Hill, California earthquake, *J. Geophys. Res.*, *93*, 6275–6296, 1988.

Bouchon, M., The state of stress on some faults of the San Andreas system as inferred from near-field strong motion data, *J. Geophys. Res.*, *102*, 11,731–11,744, 1997.

Bouchon, M., H. Sekiguchi, K. Irikura, and T. Iwata, Some characteristics of the stress field of the 995 Hyogo-ken Nanbu (Kobe) earthquake, *J. Geophys. Res.*, *103*, 24,271–24,282, 1998.

Carlson, J., and J. Langer, Mechanical model of an earthquake fault, *Phys. Rev. A*, *40*, 6470–6484, 1989.

Clayton, R. W., and B. Engquist, Absorbing boundary conditions for acoustic and elastic wave equations, *Bull. Seismol. Soc. Am.*, *67*, 1529–1540, 1977.

Cochard, A., and R. Madariaga, Dynamic faulting under rate-dependent friction, *Pure Appl. Geophys.*, *142*, 419–445, 1994.

Cochard, A., and R. Madariaga, Complexity of seismicity due to highly rate-dependent friction, *J. Geophys. Res.*, *101*, 17,581–17,596, 1996.

Day, S. M., Three-dimensional simulation of spontaneous rupture: the effect of non-uniform prestress, *Bull. Seismol. Soc. Am.*, *72*, 1881–1902, 1982.

Dieterich, J. H., Preseismic fault slip and earthquake prediction, *J. Geophys. Res.*, *83*, 3940–3946, 1978.

Dieterich, J. H., D. W. Barber, G. Conrad, and Q. A. Gorton, Preseismic slip in a large scale friction experiment, *Proc. U.S. Symp. Rock Mech.*, *19*, 110–117, 1978.

Fukuyama, E., and R. Madariaga, Rupture dynamics of a planar fault in a 3D elastic medium: Rate-and slip-weakening friction, *Bull. Seismol. Soc. Am.*, *88*, 1–17, 1998.

Fukuyama, E., and R. Madariaga, Dynamic propagation and interaction of a rupture front on a planar fault, *Pure Appl. Geophys.*, *157*, 1959–1979, 2000.

Fukuyama, E., and T. Mikumo, Dynamic rupture analysis: Inversion for the source process of the 1990 Izu-Oshima, Japan, earthquake (M = 6.5), *J. Geophys. Res.*, *98*, 6529–6542, 1993.

Graves, R. W., Simulating seismic wave propagation in 3D elastic media using staggered-grid finite differences, *Bull. Seismol. Soc. Am.*, *86*, 1091–1106, 1996.

Guatteri, M., Inferring fault rupture dynamics from strong motion data, Ph.D. thesis, Stanford Univ., Stanford, Calif., 2001.

Guatteri, M., and P. Spudish, What can strong-motion data tell us about slip-weaken fault-friction laws?, *Bull. Seismol. Soc. Am.*, *90*, 98–116, 2000.

Hartzell, S. H., and T. H. Heaton, Inversion of strong ground motion and teleseismic waveform data for the fault rupture history of the 1979 Imperial Valley, California earthquake, *Bull. Seismol. Soc. Am.*, *73*, 1553–1583, 1983.

Husseini, M. I., D. B. Jovanovich, M. J. Randall, and L. B. Freund, The fracture energy of earthquakes, *Geophys. J. R. Astron. Soc.*, *43*, 367–385, 1975.

Ida, Y., Cohesive force across the tip of a longitudinal-shear crack and Griffith's specific surface energy, *J. Geophys. Res.*, *77*, 3796–3805, 1972.

Ide, S., and M. Takeo, Determination of constitutive relations of fault slip based on seismic wave analysis, *J. Geophys. Res.*, *102*, 27,379–27,391, 1997.

Ide, S., M. Takeo, and Y. Yoshida, Source process of the 1995 Kobe earthquake: determination of spatiotemporal slip distribution by Bayesian modeling, *Bull. Seismol. Soc. Am.*, *86*, 547–566, 1996.

Iwata, T., H. Sekiguchi, Y. Matsumoto, H. Miyake, and K. Irikura, Source process of the 2000 western Tottori Prefecture earthquake and near-source strong ground motion, paper presented at 2000 Fall Meeting, Seismol. Soc. of Jpn., Tsukuba, 20 –22 Nov. 2000a.

Iwata, T., H. Sekiguchi, and A. Pitarka, Source and site effects on strong ground motions in near-source area during the 1999 Chi-Chi, Taiwan, earthquake, *Eos Trans. AGU*, *81*(48), Fall Meet. Suppl., Abstract S72B-07, 2000b.

Madariaga, R., K. B. Olsen, and R. Archuleta, Modeling dynamic rupture in a 3-D earthquake model, *Bull. Seismol. Soc. Am.*, *88*, 1182–1197, 1998.

Marone, C., and C. H. Scholz, The depth of seismic faulting and the upper transition from stable to unstable slip regimes, *Geophys. Res. Lett.*, *15*, 621–624, 1988.

Mikumo, T., E. Fukuyama, K. B. Olsen, and Y. Yagi, Stress-breakdown time and critical weakening slip inferred from the slip-velocity functions on earthquake faults, *Bull. Seismol. Soc. Am.*, *93*, 264–282, 2003.

Miyatake, T., Computer simulation of strong ground motion near a fault using dynamic fault rupture modeling: Spatial distribution of the peak ground velocity vectors, *Pure Appl. Geophys.*, *157*, 2063–2081, 2000.

Oglesby, D. D., R. J. Archuleta, and S. Nielsen, Dynamics of dip-slip faulting: Explorations in two dimensions, *J. Geophys. Res.*, *1051*, 13,643–13,653, 2000.

Ohnaka, M., Nonuniformity of crack-growth resistance and breakdown zone near the propagating tip of shear crack in brittle rock: A model for earthquake nucleation to dynamic rupture, *Can. J. Phys.*, *68*, 1071–1083, 1990.

Ohnaka, M., A physical scaling relation between the size of an earthquake and its nucleation zone size, *Pure Appl. Geophys.*, *157*, 2259–2282, 2000.

Ohnaka, M., and L. F. Shen, Scaling of the shear rupture process from nucleation to dynamic propagation: Implications of geometric irregularity of the rupturing surfaces, *J. Geophys. Res.*, *104*, 817–884, 1999.

Ohnaka, M., and T. Yamashita, A cohesive zone model for dynamic shear faulting based on experimentally inferred constitutive relation and

strong motion source parameters, *J. Geophys. Res.*, *94*, 4089–4104, 1989.

Okubo, P. G., and J. H. Dieterich, Effects of physical fault properties on frictional instabilities produced on simulated faults, *J. Geophys. Res.*, *89*, 5817–5827, 1984.

Olsen, K. B., R. Madariaga, and R. J. Archuleta, Three-dimensional dynamic simulation of the 1992 Landers earthquake, *Science*, *278*, 834–838, 1997.

Peryrat, S., K. Olsen, and P. Madariaga, Landers earthquake, *J. Geophys. Res.*, *106*, 26,467–26,482, 2001.

Pitarka, A., 3D elastic finite-difference modeling of seismic motion using staggered grids with nonuniform spacing, *Bull. Seismol. Soc. Am.*, *89*, 54–68, 1999.

Pulido, N., and K. Irikura, Estimation of dynamic rupture parameters from the radiated seismic energy and apparent stress, *Geophys. Res. Lett.*, *27*, 3945–3948, 2000.

Quin, H., stress drop and rupture dynamics of the October 15, 1979 Imperial Valley, California, earthquake, *Tectonophysics*, *175*, 93–117, 1990.

Scholz, C. H., The critical slip distance from seismic faulting, *Nature*, *336*, 761–763, 1988.

Sekiguchi, H., K. Irikura, and T. Iwata, Fault geometry at the rupture termination of the 1995 Hyogo-ken Nanbu earthquake, *Bull. Seismol. Soc. Am.*, *90*, 117–133, 2000.

Wald, D. J., and T. H. Heaton, Spatial and temporal distribution of slip for the 1992 Landers, California, Earthquake, *Bull. Seismol. Soc. Am.*, *84*, 668–691, 1994.

Yoshida, S., K. Koketsu, B. Shibazaki, T. Sagiya, T. Kato, and Y. Yoshida, Joint inversions of near-and far-field waveforms and geodetic data for the rupture process of the 1995 Kobe earthquake, *J. Phys. Earth*, *44*, 437–454, 1996.

Zhang, W. B., T. Iwata, and K. Irikura, The characteristics of the dynamic source parameters of the 2000 Tottori-Ken Seibu, earthquake, paper presented at Fall Meeting, Seismol. Soc. of Jpn., Kakoshima, 24 –26 Oct. 2001.

M. Bouchon, Universite Joseph Fourier, Laboratoire de Geophysique Interne et Tectonophysique, BP 53, 38041 Grenoble, France. (michel.bouchon@obs.ujf-grenoble.fr)

K. Irikura, T. Iwata, and W. Zhang, Strong Motion Seismology, Disaster Prevention Research Insitute, Kyoto University, Gokasho, Uji, Kyoto 611-0011, Japan. (irikura@egmdpri01.dpri.kyoto-u.ac.jp; iwata@egmdpri01.dpri.kyoto-u.ac.jp; wenbo@egmdpri01.dpri.kyoto-u.ac.jp)

H. Sekiguchi, Active Fault Research Center, Geological Survey of Japan, AIST, Site, Higashi 1-1-1, Tsukuba 305–8567, Japan. (haruko.sekiguchi@aist.go.jp)